CHEMISTRY & BIODIVERSITY

Accepted Article

Title: Design, synthesis, molecular docking, and biological evaluation of new emodin anthraquinone derivatives as potential antitumor substances

Authors: Yuying Li, Fang Guo, Tinggui Chen, Liwei Zhang, Zhuanhua Wang, Qiang Su, and Liheng Feng

To be cited as: *Chem. Biodiversity* 10.1002/cbdv.202000328

Link to VoR: https://doi.org/10.1002/cbdv.202000328

10.1002/cbdv.202000328

Design, synthesis, molecular docking, and biological evaluation of new emodin anthraquinone derivatives as potential antitumor substances

Yuying Li*, Fang Guo, Tinggui Chen, Liwei Zhang, Zhuanhua Wang, Qiang Su, Liheng Feng

Key Laboratory for Chemical Biology and Molecular Engineering of Ministry of Education, Institute of Biotechnology, Shanxi University, Taiyuan, 030006, China

*Corresponding author.

E-mail address: lyy9030@sxu.edu.cn (Y. Li)

Abstract

The emodin anthraquinone derivatives are generally used in traditional Chinese medicine due to their various pharmacological activities. In the present study, a series of emodin anthraquinone derivatives have been designed and synthesized among which 1,3-Dihydroxy-6,8-dimethoxy -9,10-anthraquinone (**11b**) is a natural compound that has been synthesized for the very first time, and 1,4-Dimethyl-6,8-dimethoxy-9,10-anthraquinone (**11c**) is a compound that has never been reported earlier. Interestingly, while total seven of these compounds showed neuraminidase inhibitory activity in influenza virus with inhibition rate more than 50%, specific four compounds exhibited significant inhibition of tumor cell proliferation. The further results demonstrate that **11c** showed the best anticancer activity among all the as synthesized compounds by inducing highest apoptosis rate to HCT116 cancer cells and arresting their G0/G1 cell cycle phase, through

elevation of intracellular level of reactive oxygen species (ROS). Moreover, the binding of **11c** with BSA protein has thoroughly been investigated. Altogether, this study suggests the neuraminidase inhibitory activity and antitumor potential of the new emodin anthraquinone derivatives.

Keywords: emodin anthraquinone derivatives, synthesis, Anti influenza virus, antitumor properties, molecular docking

Introduction

Since ancient ages, many medicinally important plants have been employed for the treatment of various diseases, throughout the world especially in Asia and Africa. The pharmacological activities of some of these plants have been well documented. [1] Various medicinal plants such as Rheum, Salamander, and Rhamnus are the key sources of different bioactive molecules, including many emodin anthraquinone derivatives such as emodin, rhein, aloe-emodin and emodin methyl ether. [2] Another emodin derivative (1,3,8-trihydroxy-6-methyl-anthraquinone) is found to be the active ingredient of Chinese traditional rhubarb, which has various pharmacological effects including antibacterial, antiviral, anti-inflammatory, liver-protective, and anti-tumor activities. [3-10] Therefore, the research on emodin derivatives has recently attracted great attention to the scientists. To comprehend the structure-activity relationship, several research groups synthesized different emodin anthraquinone derivatives employing naturally extracted emodin as raw material and investigated their potential activities. For instance, Steffi K and research group used halogenated emodin as a raw material to fabricate emodin derivatives, which were capable of inhibiting ATP citrate lyase. [11] Similarly, Yang K and team developed a series of lead compounds with antitumor

activity employing emodin as a raw material. [12]

Recent studies have reported that emodin can induce apoptosis, cell migration inhibition and cell cycle arrest in a variety of tumor cells (lung and liver cancer). [12-14] Although emodin derivatives are present in many plants, their practical applications for cancer therapy are associated with several factors such as their low content in plants, complicated extraction process, and limitation of active screening. [1] Therefore, it is urgently required to focus on the total synthesis of emodin derivatives along with the modification of their structure to find novel anticancer drugs with better efficacy and less toxicity.

In the present study, a series of emodin anthraquinone derivatives has been synthesized by combining the principle and mechanism of antitumor drugs with the structure-activity relationship of anthraquinone derivatives. After through biological screening, several anthraquinone compounds have been found to exert neuraminidase inhibitory activity in influenza virus and antitumor activity toward HCT116 colon cancer cells. Among these anthraquinone compounds, the natural product **11b** (1,3-dihydroxy-6,8-dimethoxy-9,10-anthraquinone) has been synthesized for the very first time, and compound **11c** (1,4-dimethyl-6,8-dimethoxy-9,10-anthraquinone) has not earlier been reported. As the compound **11c** exhibited the best better anticancer activity among all the as synthesized compounds toward HCT116 cells, **11c** was employed for subsequent mechanistic studies. The results demonstrated that **11c** treatment could enhance the level of intracellular reactive oxygen species (ROS) in HCT116 cells, leading to induction of apoptosis and cell cycle arrest in G0/G1 phase. Furthermore, the binding of **11c** with BSA protein has been studied employing fluorescence titration and CD spectroscopy, followed by molecular docking. Overall, this study suggests that the emodin anthraquinone derivatives could be beneficial for the

treatment of different virus mediated diseases and cancers in near future.

Result and Discussion

Chemistry

Synthesis of a series of anthraquinone derivatives

To date, anthraquinone derivatives can be synthesized mainly through two steps of Friedel-crafts reaction and cyclization process. [15,16] Mugunthu RD and co-workers reported the synthesis of anthraquinone derivatives in the molten state of aluminum trichloride and sodium chloride (2:1), using phthalic anhydride and substituted benzene derivatives as the raw materials. [17] The above synthetic methods have several disadvantages including harsh reaction conditions, long reaction time, as well as low yield. To overcome these limitations, in the present study, anthraquinone derivatives (**3a-3h**) have been synthesized employing microwave assisted one step process, using phthalic anhydride and substituted benzene derivatives as the raw materials, and $AlCl_3$/PPA or $AlCl_3/H_2SO_4$ as catalysts (*Scheme 1*). The obtained compounds have thoroughly been characterized by different spectroscopic techniques including UV, IR, ^{1}H NMR and EI-MS.

Scheme 1. Synthesis of a series of anthraquinone derivatives

Synthesis of emodin anthraquinone derivatives

To synthesize emodin anthraquinone derivatives, the raw material methyl 3,5-dimethoxybenzoate was first reacted with chloral hydrate. Further 3,5-dimethoxyphthalic anhydride was synthesized employing a series of reactions such as alkylation, transesterification, hydrolysis, and decarboxylation. A series of emodin anthraquinone derivatives (**11a-11b**) were then synthesized through the interaction of 3,5-dimethoxyphthalic anhydride and different substituted benzenes under microwave assisted heating, where $AlCl_3/H_2SO_4$ was used as a catalyst. The corresponding

synthetic route is presented in *Scheme 2*.

During synthesis of the anthraquinone derivative **11a**, a conventional heating involving two steps was used at the beginning. At first, Friedel-Crafts reaction was performed using CS_2, CCl_4, and CH_2Cl_2 as solvents. The effect of CS_2 was found to be better with higher yield as compared to the other solvents. However, during cyclization, it was found that the use of concentrated sulfuric acid/boric acid, oleum/boric acid or polyphosphoric acid (PPA) led to higher reaction temperature, which was not easy to control. According to published literature, when the reaction temperature is higher than 100 °C, the oxymethyl group can be cleaved to form a hydroxyl group. [18] Therefore, during the synthesis of compound **11a**, all of its methoxy groups were cleaved to form 1,3,5,8-Tetrahydroxy-2-methyl-anthraquinone with low yield. However, after the microwave reaction, the methoxy cleavage of the latter two compounds became very weak, and hence the yield was also increased. Nonetheless, the amplitude was not large, which could be attributed to the influence of the phthalic anhydride substituent.

Scheme 2. Synthesis of 3,5-Dimethoxy-phthalic anhydride and emodin anthraquinone derivatives.

Synthesis of a series of amide anthraquinone derivatives

As show in *Scheme 3*, a series of new amide anthraquinone derivatives have been synthesized. The compound 13 (1-Nitro-2-methyl-anthraquinone) was first fabricated by nitration reaction employing 2-methylanthraquinone as a raw material, followed by reduction process to obtain the compound 14 (1-amino-2-methylanthraquinone). Finally the compounds **15**a and **15**b were obtained by acylation. In addition, compound 16 (1-Nitro-2-carboxy-anthraquinone) was synthesized by oxidation of $Na_2Cr_2O_7$, and then the nitro group at position 1 was converted to

amino group through reduction to obtain the compound **17**.

Scheme 3. Synthesis of anthraquinone derivatives

Biology

Biological activity of anthraquinone derivatives

The anthraquinone derivatives have thoroughly been screened to evaluate their neuraminidase inhibitory activity in influenza virus (NA). To check this activity, the compounds were allowed to interact with a fluorescent substrate MUNANA under the catalysis of influenza virus neuraminidase, and the decrease in fluorescence intensity of the metabolite was measured at 450 nm. *Table 1*, demonstrates that the compounds **11a**, **11c**, **11d**, **11c**, **11e**, **11f**, and **17** could efficiently inhibit the neuraminidase activity with inhibition rate more than 50%. Among these seven compounds, **11a** exerted the highest neuraminidase inhibitory activity, with an IC_{50} value of 96.1 μM. Aloin, (10-β-D-Glucopyranosyl-1,8-dihydroxy-3-(hydroxymethyl)-9(10H)anthracenone), has good anti-influenza virus activity in vivo and in vitro, and its anti-influenza virus mechanism is also the same as inhibition of neuraminidase, IC_{50} value is 100 μM. Compared with aloin, **11a** has similar activity, which proves that **11a** has relatively strong anti-influenza virus activity. [19]

Further the structural analysis indicated that the difference between the compounds **11c** and **3c** was only the methoxy modification at the R position in **11c**. However, these modification could enhance the neuraminidase inhibitory effect of **11c** as observed by the lower IC_{50} value of **11c** (IC_{50} = 108.1 μM) as compared to that of **3c** (IC_{50}=157.2 μM). Contrastingly, the structural difference between **3e** and **3f** was the methyl substitution at R_2 position in **3f**, which led to the higher IC_{50} value of **3e** (IC_{50} = 129.1 μM) than that of **3f** (IC_{50} = 100.0 μM), with enhanced activity. In addition, compound **17** with amino and carboxyl groups at the positions of R1 and R2,

10.1002/cbdv.202000328

respectively exhibited enhanced neuraminidase inhibitory activity. Therefore, it can be suggested that the structural modification on R1 and R2 can increase the inhibitory activity of these compounds to neuraminidase. However, the structural modification of the compounds on R was not conducive to increase their inhibitory activity.

Table 1. Neuraminidase inhibitory activity of anthraquinone derivatives.

Compound	R	R1	R2	R3	R4	Inhibition ratio (%)	IC_{50} (μM)
11a	OH	OH	CH_3	OH	H	67.86	96.1
11c	OCH_3	CH_3	H	H	CH_3	50.55	108.1
11d	OCH_3	OH	H	H	H	61.26	113.1
3c	H	CH_3	H	H	CH_3	53.80	157.2
3e	H	OH	H	OH	H	61.49	129.1
3f	H	OH	CH_3	OH	H	75.06	100.0
17	H	NH_2	COOH	H	H	61.06	108.1

These synthesized anthraquinone derivatives have also been screened to check their antitumor potential, besides the evaluation of their inhibitory activity to neuraminidase. The anthraquinone derivatives have been administered to eight different kinds of tumor cells (HepG2, EC9706, SW480, QBC-939, HeLa, SGC-7901, MCF-7, and HCT116) and one type of normal intestinal epithelial cells (FHC), followed by determination of cell viability using MTT reagent. After thorough screening, it was found that the compounds **11a-11d** inhibited the proliferation of tumor cells without exerting any cytotoxicity to the normal cells (IC_{50}>1000 μM), suggesting their potential antitumor activities (*Table 2*). The result exhibits that the compound **11a** had the strongest inhibitory effect on EC9706 cell proliferation with IC_{50} value of 172.8 μM and SI value of 6.7. Contrastingly, the compound **11b** demonstrated its strongest anti-proliferative effect toward HepG2 cells with IC_{50} value of 144 μM and SI value of 6.6. While the compound **11c** significantly inhibited the proliferation of HCT116 cells with IC_{50} value of 108.1 μM and SI value of 10.9, the

compound **11d** exhibited the strongest anti-proliferative effect toward HepG2 cells with IC_{50} value of 241.5 μM and and SI value of 2.9. Nonetheless, the antitumor effect of **11d** was not as good as the other three compounds. In addition, it is reported in the literature that the IC_{50} value of rhein for inhibiting SW480 cell proliferation is 130 μM. [20] **11c** inhibited the proliferation of this cell with an IC_{50} value of 118.9 μM. The activity of **11c** is significantly enhanced compared to rhein. The compound **11c** was found to induce the highest antitumor effect as compared to the other compounds to most of the cancer cells, especially toward HCT116 cells (IC_{50}=108.1 μM). Therefore, the further mechanistic studies were performed with the compound **11c** to explicate the mechanism of anticancer activities of anthraquinone derivatives in HCT116 cells.

Table 2. Emodin anthraquinone derivatives inhibit tumor cell proliferation.

	HepG2		EC9706		SW480		QBC-939		HeLa		SGC-7901		MCF-7		HCT116	
	IC_{50}[b]	SI	IC_{50}[b]	SI	IC_{50}[b]	SI	IC_{50}[b]	SI	IC_{50}[b]	SI	IC_{50}[b]	SI	IC_{50}[b]	SI	IC_{50}[b]	SI
11a	181.1	6.4	172.8	6.7	185.8	6.3	242.2	4.8	222.8	5.2	260.4	4.5	193.3	6.0	189.6	6.1
11b	144.0	6.6	225.7	4.2	202.7	4.7	257.0	3.7	167.0	5.6	203.7	4.3	153.7	6.1	182.0	5.2
11c	115.9	10.2	111.5	10.6	118.9	9.9	238.2	5.0	120.9	9.8	204.4	5.8	135.1	8.8	108.1	10.9
11d	241.5	2.9	244.4	2.9	261.3	2.7	282.4	2.5	265.5	2.7	305.6	2.3	257.0	2.7	267.6	2.6

[a] Use normal intestinal epithelial cells (FHC) as a control

[b] IC_{50} value unit is micromolar (μM).

*Cell viability in HCT116 and FHC cells administered with the compound **11c***

Previous studies demonstrated that emodin can inhibit tumor cell proliferation. However, the antitumor potential of the compound **11c** has not earlier been reported. [21] In the present study, the cell viability assay was performed employing MTT reagent in both cancerous (HCT116) as well as non-cancerous (FHC) cells, incubated with the compound **11c,** relative molecular mass 296, (0, 25, 50, 100 μg/mL) for 24 h. *Figure 1,A 1,B* demonstrate that the compound **11c** significantly inhibited the proliferation of HCT116 cells as compared to the untreated control experiment in a

concentration dependent manner. However, the compound **11c** treatment could not alter the cell viability of FHC cells significantly in comparison with the untreated control experiment. These results suggest the potential antitumor activity of this anthraquinone derivative.

Figure 1. Cell viability assay in HCT116 and FHC cells using MTT reagent. The effect of **11c** treatment (0, 25, 50, 100 μg/mL, 24 h) on the viability of *A)* HCT116 cells and *B)* FHC cells. * p <0.05, ** p <0.01 as compared to the control group were considered as significantly different.

Apoptosis analysis in HCT116 cells using flow cytometry and western blot analysis

Apoptosis, referring to a method of programmed cell death, controls the occurrence and development of tumor cells. Earlier study demonstrated that the emodin anthraquinone compounds can induce apoptosis to tumor cells leading to cell death. [22] Therefore, after detecting the efficient anti-proliferative effect of **11c** toward HCT116 cells, further mechanistic studies was carried out to comprehend whether the apoptosis process was involved in **11c**-induced cancer cell death. *Figure 2,A 2,B* (flow cytometry data) exhibits that the compound **11c** treatment significantly induced apoptosis in HCT116 cells in a dose dependent fashion (apoptotic cell: 20.4% for 25 μg/mL dose; 36.7% for 50 μg/mL dose) as compared to the control experiment (apoptotic cell: 4.8%). To confirm this result, western blot analysis was further performed in HCT116 cells treated with compound **11c** for checking the expression of apoptosis-related proteins including Bax, Bcl-2, Cleaved caspase 3, and Cleaved caspase 9. As shown in *Figure 2,C 2,D*, while **11c** treatment upregulated the expression of apoptotic protein Bax, it could downregulate the expression of anti-apoptotic protein Bcl-2 in a dose dependent manner as compared to the untreated control experiment. Moreover, **11c** treatment also led to dose dependent upregulation of the expressions of Cleaved caspase 3 and Cleaved caspase 9 in comparison with the untreated control cells. The

western blot analysis clearly suggests that the compound **11c** induced cancer cell death through apoptosis.

Figure 2. The compound **11c** induces apoptosis to HCT116 cells in a dose-dependent manner. *A)* Flow cytometry was used to detect the apoptosis of HCT116 cells incubated with **11c** (0, 25, 50 μg/mL, 24 h). *B)* According to the results of flow cytometry, the apoptotic histogram was prepared. The experiment was repeated thrice. * p <0.05 and ** p <0.01 as compared to control group were considered as significantly different *C)* Western Blot was performed in HCT116 cells treated with compound **11c** (0, 25, 50 μg/mL, 24 h) to check the expression of apoptosis-related proteins. *D)* A grayscale analysis was performed based on the results of the western blot to obtain a histogram. The experiment was repeated thrice. * p <0.05 and ** p <0.01 as compared to control group were considered as significantly different.

Cell cycle analysis in HCT116 cells using flow cytometry

To explicate further mechanism of cancer cell death induced by compound **11c**, cell cycle analysis was performed in HCT116 cells using flow cytometry. The result exhibits that **11c** treatment led to increase the cell population in G0/G1 phase in a dose dependent fashion (cell population: 55.39% for 25 μg/mL dose; 60.31% for 50μg/mL dose) with subsequent decrease of cell population in G2/ M and S phases as compared to the untreated control cells (*Figure 3,A 3,B*). This study suggests that **11c** treatment could arrest the G0/G1 cell cycle phase of HCT116 cancer cells, leading to apoptosis process.

Figure 3. The treatment of compound **11c** led to cell cycle arrest in G0/G1 phase of HCT116 cells. *A)* HCT116 cell cycle arrest was detected by flow cytometry upon treatment with the compound **11c** (25-50 μg/mL, 24 h). *B)* Histogram analysis showing the cell distribution in different phases

of cell cycle. The experiment was repeated thrice. * p <0.05 and ** p <0.01 as compared to control group were considered as significantly different.

Determination of intracellular ROS level in HCT116 cells

The earlier literature reported that excessive production of intracellular ROS causes oxidative stress, leading to apoptosis induction to a variety of tumor cells, including colon cancer cells. [23] In addition, previous reports exhibited that emodin can reverse the apoptosis of gastric cancer cells through addition of ROS scavengers. [24] Therefore, in the present study, the production of intracellular ROS was investigated in HCT116 cells upon treatment with the compound **11c**. *Figure 4,A 4,B* depict that **11c** treatment enhanced the number of DCFH-DA positive cells in a dose dependent manner (829.44 for 25 μg/mL; 1174.48 for 50 μg/mL) as compared to the control experiment. This result indicates that **11c** can induce the intracellular production of ROS in HCT116 cells, which could be one of plausible mechanisms behind the antitumor activity of the anthraquinone derivative.

Figure 4. The treatment of **11c** enhances the ROS level in HCT116 cells. *A)* Determination of ROS production in HCT116 cells treated with **11c** (0, 25, 50 μg/mL, 24 h) using flow cytometry. *B)* A corresponding bar graph based on the fluorescence values. The experiment was repeated thrice. * p <0.05 and ** p <0.01 as compared to control group were considered as significantly different.

*Interaction between **11c** and BSA*

Fluorescence spectroscopy, possessing higher accuracy and specificity as compared to UV-visible spectroscopy, is an important method to study the interaction of biological macromolecules with various organic small molecules, ions and inorganic compounds.[25] Common serum albumins include human serum albumin and bovine serum albumin, which are involved in various

10.1002/cbdv.202000328

transportation and regulation of the body system. [26] The interaction of a compound with BSA can enhance its solubility and dispersibility during blood transport. [27] Based on the importance of BSA in pharmacokinetics, the interaction between the compound **11c** and BSA was further studied using fluorescence titration, which would be helpful to better understand the role of emodin-BSA binding complexes for the *in vivo* applications of emodin anthraquinone derivatives.

It is well known that the endogenous fluorescence of BSA is formed by a combination of fluorescence from tyrosine, tryptophan, as well as phenylalanine. [28] Keeping the concentration of BSA unchanged, the same volume of **11c** solution with different concentrations, was added in order, followed by scanning the fluorescence spectrum of the mixed solution system sequentially. As shown in *Figure 5,A*, with increase in concentration of **11c**, the fluorescence intensity of the solution system was regularly quenched and the emission peaks exhibited a slight red shift. This result proves that with the addition of **11c**, the microenvironment of BSA was altered significantly leading to reduce its hydrophobicity, disintegrate its internal hydrophobic structure, and enhance the degree of peptide chain extension. It can be speculated that the compound **11c** could easily enter into the hydrophobic cavity of BSA and further interact with the hydrophobic amino acid residues. **11c** could approach the hydrophobic cavity through electrostatic attraction, which might affect the conformational change of BSA, leading to quenching of the endogenous fluorescence of BSA.

Fluorescence quenching could be of two types namely, dynamic quenching and static quenching. It was initially assumed that **11c** mediated BSA fluorescence quenching is involved dynamic quenching. The Stern-Volmer equation for dynamic quenching is:

$$F_0/F=1+K_q\tau_0[Q]=1+k_{sv}[Q]$$ [29] [1]

In the formula, F_0 and F refer to the fluorescence intensities in absence and presence of the quencher Q. Kq is the rate constant of the bimolecular quenching process and τ_0 is the average life of the biological macromolecules in absence of the quencher. k_{sv} refer to the dynamic quenching constant.

Using S0-F to [Q] as a Sern-Volmer plot, the results are presented in *Figure 5,B*. Based on the slope of the fitted straight line, the quenching constant k_{sv} of **11c** to BSA was calculated to be 1.1 × 10^4 L/mol, and the linear correlation coefficient was R = 0.9982. Previous reports demonstrated that the fluorescence lifetime of biological macromolecules is about 10^{-8} s, and the maximum diffusion collision quenching rate constant of different quenchers for biological macromolecules is 2.0 × 10^{10} L / (mol • s). The **11c**-BSA fluorescence quenching rate constant was found to be 1.1 × 10^{12} L / (mol • s), which is much larger than the abovementioned maximum diffusion collision quenching rate constant. This result indicates that the quenching of BSA fluorescence by **11c** is a static quenching.

In the serum albumin protein molecule, tryptophan, tyrosine and phenylalanine residues have strong absorption peaks at 230-310 nm. Therefore, CD spectra was employed to study the conformational changes of serum albumin upon interacting with the compound **11c**. As shown in *Figure 5,C*, BSA exerted a negative Cotton effect at 223 nm, which was contributed by the alpha helix structure in the BSA. After the addition of **11c**, the negative Cotton effect of BSA was weakened. However, the shape of the CD spectrum did not alter and a red shift was observed. This phenomenon could be attributed to the hydrophobic effect of the compound or the increased β-sheet structure. This result suggests that the combination of **11c** and BSA caused a significant impact on the secondary structure of BSA. The compound **11c** could destroy the α-helix structure

of BSA through hydrophobic interaction as well as hydrogen bonding interaction, leading to a decrease in the α-helix content in the structure of BSA.

Figure 5. Interaction between the compound **11c** and BSA A) Compound **11c** quenched the fluorescence of BSA. $C_{BSA}=1.0\times10^{-6}$ mol/L; $C_{11c}=1.0\times10^{-4}$ mol/L; T=297K B) Stern-Volmer fluorescence quenching curve of **11c** versus BSA system. C) The effect of **11c** on the CD spectrum of BSA. $C_{BSA}=1.0\times10^{-6}$ mol/L; $C_{11c}=1.0\times10^{-4}$ mol/L; T=298.15K

Molecular docking studies

Molecular docking is one of the most useful tools for studying the interaction between proteins and organic molecules. Molecular docking studies can easily confirm the results of previous experiments.[30] Therefore, docking analysis was performed employing AutoDock 4.2.6 software to investigate the interaction between compound **11c** and BSA protein. As the binding site of **11c** and BSA was previously unknown, the compound **11c** was first put into the crystal structure of BSA to allow free binding, and it was observed that **11c** could finally bind to the cavity on the A chain of BSA (*Figure 6*). In addition, the hydrogen bonding interaction between **11c** and BSA was also analyzed. As shown in *Figure 6,B*, using Automatic the total score was 1.9599, and three hydrogen bonds were formed by tightly binding with amino acid residues ARG435 and LYS431. Subsequently, the hydrophobicity of **11c** was explored through molecular docking as shown in *Figure 6,B*. Here, the blue color referred to the hydrophilic site of BSA, while the green color indicated its hydrophobic site. It can be clearly observed that the combination of **11c** with the hydrophobic cavity of BSA can interact with hydrophobic amino acid residues, suggesting that **11c** is hydrophobic in nature. This data corroborates with the earlier fluorescent titration results that the compound **11c** could alter the microenvironment especially the hydrophobicity of BSA. The

secondary structure of **11c** and BSA was further analyzed and presented in *Figure 6,D*. The result exhibits that the compound **11c** entered into the position of α-helix of the A chain in BSA. From the results of CD spectra, it can be clearly observed that the combination of **11c** and BSA caused the conformational changes in of BSA. This phenomenon led to the destruction of α-helix structure of BSA through hydrogen bonding interaction and hydrophobic interaction, which is in agreement with the docking result.

Figure 6. Molecular docking between **11c** and BSA molecules. *A)* Binding of **11c** with BSA. *B)* **11c** forms hydrogen bonds with BSA. *C)* **11c** can bind to BSA hydrophobic site. *D)* Binding of **11c** with secondary structure of BSA.

Conclusion

In conclusion, we designed and synthesized a series of new emodin anthraquinone derivatives, followed by their characterizations. After thorough biological screening, it was observed that seven anthraquinone compounds could inhibit the neuraminidase activity of influenza virus with inhibition rate more than 50%. Moreover, four of these compounds especially **11c** inhibited the proliferation of cancer cells significantly without showing any cytotoxicity to normal cells, suggesting their potential antitumor activity. The mechanistic studies showed that the compound **11c** treatment can elevate the intracellular level of ROS in HCT116 cells, leading to induction of apoptosis and cell cycle arrest in the G0/G1 phase. In addition, the binding studies using fluorescence titration and CD spectroscopy exhibited that the combination of **11c** and BSA caused a significant impact on the secondary structure of BSA. The compound **11c** could destroy the α-helix structure of BSA through hydrophobic interactions and hydrogen bonding interactions, which corroborate with the molecular docking analysis. Overall, this study offers the basis for

further development of anthraquinone derivatives for various biological applications.

Experimental Section

Materials

The synthesis and characterizations were performed employing chemical microwave reactor (Nanjing Lingjiang Technology, China), IR spectrum (Perkin elmer, Japan), UV-2000 (UNICO, Shanghai), and DRX-300 (300Hz) nuclear magnetic resonance instrument (Bruker Biospin, Switzerland). All the reagents used in the experiments were purchased and utilized directly without further purification. The deuterated $CDCl_3$, DMSO and tetramethylsilane were procured from Energy Chemical, China. GF 254 silica gel plate was purchased from Shandong Qingdao Chemical Industry, China. While RPMI-1640 medium was obtained from HyClone, USA, fetal bovine serum (FBS) was procured from Sangon Biotechnology, Shanghai. MTT was purchased from Sigma, USA. While Annexin V-FITC assay kit was obtained from Pharmingen-Becton Dickinson, USA, the Cell Cycle Detection Kit was procured from KeyGen Biotech, Nanjing. The primary antibodies (e.g. Bcl-2, Bax, Cleaved caspase-3, and Cleaved caspase-9), and ROS detection kit were purchased from Beyotime Biotechnology, China. Horseradish peroxidase-labeled goat anti-rabbit IgG secondary antibody, and β-actin antibody primary antibody were procured from Bioworld, USA. While, ECL luminescence assay kit was obtained from Engreen Biosystem, China, BCA protein quantification kit was purchased from Minbio, china. PVDF membrane was procured from Millipore, Germany. Bovine serum albumin was purchased from Solarbio, Beijing.

Methods

Screening of anthraquinone derivatives for the neuraminidase inhibitory activity in influenza virus.

A certain concentration of the test compounds and influenza virus neuraminidase (NA) were suspended in a reaction buffer (pH 6.5), and a fluorescent substrate 2'-4-methylumbelliferyl-α-N-acetylneuraminate (MUNANA) was added into the reaction system, followed by incubation for 60 min, at 37˚C. The reaction was then stopped by adding a reaction stop solution. Next, the fluorescence intensity was measured at an excitation wavelength of 360 nm and an emission wavelength of 450 nm. It is to be mentioned here that the fluorescence intensity of the reaction system can directly reflect the enzyme activity. Therefore the NA inhibitory activity of the test compounds can be calculated from the decrease in fluorescence intensity.

Cell culture. Human colon cancer cell line HCT116, normal intestinal epithelial cell line FHC, human cervical cancer cell line HeLa, human breast cancer cell line MCF-7, human bile duct cancer cell line QBC-939, human liver cancer cell line HepG2, human gastric cancer cell line SGC-7901 and human colorectal cancer cell line SW480 were purchased from Cell Bank of the Chinese Academy of Sciences (Shanghai, China). The human esophageal cancer cell line EC9706 was obtained by Prof. Ming Rong Wang, Chinese Academy Medical of Sciences from Cancer Hospital Institute. While EC9706, HeLa and SW480 cells were cultured in RPMI 1640 medium containing 10% (v/v) heat-inactivated fetal calf serum (FCS), MCF-7, QBC-939, SGC-7901 and HepG2 cells were cultured in DMEM medium containing 10% FBS, 100 U/mL penicillin and 100 U/mL streptomycin. The above cells were cultured inside a humidified cell incubator with 5% CO_2 at 37 °C.

Preparation of stock solutions. The test compounds were soluble in DMSO. Therefore, they were dissolved in DMSO at a concentration of 10^{-4} mol/L to prepare the respective stock solutions,

which were further diluted to the required concentration with the corresponding cell culture medium for all the experiments.

Cell viability test. The cells were seeded at a density of 1×10^5 cells/mL in a volume of 100 μL media into each well of 96-well microtiter plate. After adherence, the cells were incubated with the test compounds (25-100 μg/mL) for 24h. The cells were then incubated with 20 μL of MTT solution (5 mg/mL) at 37 °C for another 4 h. After removing the culture medium and containing MTT solution, 150 μL of DMSO was added to each well and the plate was placed on a shaker at room temperature for around 5 min. The absorbance was measured using a microplate reader at 490 nm. The average absorbance of three parallel experiments was calculated using the following formula:

Percent inhibition = 1- (average experimental absorbance/average control absorbance) × 100% [2]

Annexin V-FITC/PI staining assay. Six-well tissue culture plates were seeded with 1×10^4 HCT116 cells per well. After adherence, the cells were incubated with the compound **11c** (25-50 μg/mL) for 24 h. The apoptosis analysis was then performed employing Annexin V-FITC/PI apoptosis detection kit. At first, the cells were resuspended in 500 μL of binding buffer containing 5 μL of annexin V-FITC and 1 μL of PI, and incubated for 30 min in the dark at room temperature. The number and distribution of apoptotic cells were then counted using flow cytometry analysis (FACSCalibur).

Cell cycle analysis. In brief, HCT116 cells were seeded into 6-well tissue culture plates and after adherence, the cells were incubated with the compound **11c** (25-50 μg/mL) for 24h. The cells were then fixed with 0.7 mL of 70% ethanol at 4 °C for overnight. Next, the fixed cells were centrifuged and washed with PBS for 30 min at room temperature under dark condition. After that,

the cells were stained with 100 μL PI (1 mM) containing 50 μL RNase A (1 mM) subjected to flow cytometer for cell cycle analysis.

Measurement of intracellular ROS. The intracellular ROS level in HCT116 cells were measured through flow cytometry, employing 2', 7'-Dichlorofluorescein-diacetate (DCFH-DA) reagent. The cells (1×10^4 cells per well) were first seeded into six-well tissue culture plates. After adherence, the cells were treated with the compound for respective time duration, followed by incubation with 1 mL of DCFH-DA(10 μM) for 30 min at 37 °C under dark condition. The stained cells were then washed thrice with PBS and further kept in 300 μL of PBS. The fluorescence intensity was measured using a flow cytometer (FACSCalibur) with 488/525 nm excitation/emission filter.

Western blot analysis. HCT116 cells were incubated with the compound **11c** for 24 h. The cells were then washed with cold PBS thrice and incubated with lysis buffer for 30 min on ice. After that, the cells were centrifuged at 12,000 × g for 15 min at 4°C, and the supernatant cell lysate was collected. The protein concentration of the obtained cell lysate was measured using a BCA protein quantification kit (Beyotime Institute of Biotechnology, Shanghai). The total protein of 60 μg was separated by 10% SDS-PAGE, followed by transfer to a PVDF membrane. The membrane was then blocked with 5% skim milk in 0.1% Tris buffer containing 0.05% Tween-20 (TBST) for 1 h at room temperature. After that, PVDF membrane was incubated with primary antibodies (anti-Bax, Bcl-2, cleaved caspase 9 and cleaved caspase 3) at 4 °C for overnight. The membrane was washed with TBST thrice, followed by incubation with HRP-conjugated secondary antibody for 1 h at room temperature. After washing the membrane again with TBST thrice, the protein bands on the membrane were detected employing an enhanced

chemiluminescence detection kit (Engreen) and exposed to X-ray film.

Docking analysis. The crystal structure of BSA with a resolution of 2.47Å (4F5S) was obtained from the Protein Data Bank (PDB) database. The water molecules in the target protein were removed using SYBYL-2.0X software. It was saved in mol2 format, and the processed BSA was hydrogenated and charged in AutoDuck Tools software. It was then molecularly docked with the compound **11c**. The affinity of BSA and **11c** was analyzed through scoring and hydrogen bonding.

Fluorescence spectroscopy. 2 mL of BSA (1.0×10^{-6} mol/L) solution was taken into 1 cm quartz cuvette and 2 μL of 10^{-4} mol/L **11c** compound solution was poured into it. The solution mixture was shaken well and kept for 5 min without disturbing. Fluorescence spectra of BSA and compound solutions were measured at room temperature. While the fluorescence excitation wavelength was fixed at λex = 251 nm, the emission wavelength was set to λem = 344 nm. The scanning speed was 250 nm/min, and the slit was 5 nm.

CD spectrometry. 2 mL of BSA (1.0×10^{-6} mol/L) solution was taken in 1 cm sample cell and 2 μL of 10^{-4} mol/L **11c** compound solution was poured into it, followed by shaking the well mix the solutions well. CD spectra of BSA and **11c** were measured at room temperature with scanning speed 1 nm/min and scanning range 210-250 nm.

Acknowledgments

This work was supported by the Key projects of Shanxi Province (No. 201903D321095) and Transformation of Scientific and Technological Achievements Programs of Higher Education

Institutions in Shanxi (TSTAP). We thank Prof. Daxiong Han from Medical College Xiamen University for software support. We would also like to thank Mr. Du Guanhua, Mr. Liu Ailin, and Mr. Hu for their assistance in the activity testing of the National Drug Screening Center of the Institute of Materia Medica, Chinese Academy of Medical Sciences.

Author Contribution Statement

Q. S. and L. F. performed the synthetic experiments and analyzed the data. F. G. and T. C. performed the biological experiments and analyzed the data. Y. L. and F. G. designed the experiments. F. G., Y. L., L.Z., Z. W. wrote/corrected the article.

Conflict of interest

The authors declare they have no conflict of interest.

Appendix A. Supplementary data

Supplementary data associated with this article can be found.

References

[1]X. Dong, Y. Zeng, Y. Liu , L. You, X. Yin, J. Fu, J. Ni, 'Aloe-emodin: A Review of its Pharmacology, Toxicity and Pharmacokinetics', *Phytother. Res.* **2020**, *34*, 270-281.

[2]B. A. Monisha, N. Kumar, A. B. Tiku, 'Emodin and Its Role in Chronic Diseases', *Adv. Exp. Med. Biol.* **2016**，*928*，47-73.

[3]X. Hou, W. Wei, Y. Fan, J. Zhang, N. Zhu, H. Hong, C. Wang, 'Study on synthesis and bioactivity of biotinylated emodin', *Appl. Microbiol. Biotechnol.* **2017**，*13*, 5259-5266.

[4]L. Li, X. Song, Z. Yin, R. Jia, Z. Li, X. Zhou, Y. Zou, L. Li, Yin L, G. Yue, et al., 'The antibacterial activity and action mechanism of emodin from Polygonum cuspidatum against Haemophilus parasuis in vitro', *Microbiol. Res.* **2016**, *186*, 139-145.

[5]S. W. Li, T. C. Yang, C. C. Lai, S. H. Huang, J. M. Liao, L. Wan, Y. J. Lin, C. W. *Lin*, 'Antiviral activity of aloe-emodin against influenza A virus via galectin-3 up-regulation', *Eur. J. Pharmacol.* **2014**, *738*, 125-32.

[6]J. W. Han, D. W. Shim, W. Y. Shin, K. H. Heo, S. B. Kwak, E. J. Sim, J. H. Jeong , T. B. Kang, K. H. Lee, 'Anti-inflammatory effect of emodin via attenuation of NLRP3 inflammasome activation', *Int. J. Mol. Sci.* **2015,** *16*, 8102-9.

[7]E. H. Lee, S. Y. Baek, J. Y. Park, Y. W. Kim, 'Emodin in Rheum undulatum inhibits oxidative stress in the liver via AMPK with Hippo/Yap signalling pathway', *Pharm. Microbiol.* **2020**，*58*，333-341.

[8]G. Dai, K. Ding, Q. Cao, T. Xu, F. He, S. Liu, W, Ju 'Emodin suppresses growth and invasion colorectal cancer cells by inhibiting VEGFR2', *Eur. J. Pharmacol.* **2019**, *15*, 172525.

[9]Y. Ding, P. Liu, Z. L. Chen, S. J. Zhang, Y. Q. Wang, X. Cai, L. Luo, X. Zhou, L. Zhao, 'Emodin Attenuates Lipopolysaccharide-Induced Acute Liver Injury via Inhibiting the TLR4 Signaling Pathway *in vitro* and *in vivo*', *Front. Pharmacol.* **2018**, *9*, 962.

[10]S. F. Chen, Z. Y. Zhang, J. L. Zhang, 'Emodin enhances antitumor effect of paclitaxel on human non-small-cell lung cancer cells in vitro and in vivo', *Drug Des. Dev. Ther.* **2019**, *13*, 1145-1153.

[11]K. Steffi, Koerner, J. Hanai, S. Bai, F. E. Jernigan, M. Oki, C. Komaba, E. Shuto, V. P. Sukhatme, L. Sun，'Design and synthesis of emodin derivatives as novel inhibitors of ATP-citrate lyase', *Eur. J. Med. Chem.* **2017**, *126*, 920-928.

[12]K. Yang, M. Jin, Z. Quan, H. Piao, 'Design and Synthesis of Novel Anti-Proliferative Emodin Derivatives and Studies on their Cell Cycle Arrest, Apoptosis Pathway and Migration', *Molecules.* **2019**, *24*, 884.

[13]X. P. Pan，C. Wang，Y. Li，L. Zhu，T. Zhang, 'Protective autophagy induced by physcion suppresses hepatocellular carcinoma cell metastasis by inactivating the JAK2/STAT3 Axis', *Life Sci.* **2018**, *214*, 124-135.

[14]N. Yang, C. Li, H. Li, M. Liu, X. J. Cai, F. J. Cao, Y. B. Feng, M. L. Li, X. B. Wang, 'Emodin Induced SREBP1-Dependent and SREBP1-Independent Apoptosis in Hepatocellular Carcinoma Cells', *Front. Pharmacol.* **2019**, *10*, 709.

[15]L. Mahesh, Patil, B. B. Hanumant,D. E. Ponde, V. H. Deshpande, 'Total synthesis of

(±)-brasiliquinone. Tetrahedron', *Tetrahedron.* **2002**, *58*, 6615-6620.

[16]S. Yeap, M. N. Akhtar, K. L. Lim, N. Abu, W. Y. Ho, S. Zareen, K. Roohani, H. Ky, S. W. Tan, N. Lajis, N. B. Alitheen, 'Synthesis of an anthraquinone derivative (DHAQC) and its effect on induction of G2/M arrest and apoptosis in breast cancer MCF-7 cell line', *Drug Des. Devel Ther.* 2015, *17*, 983-992.

[17]M. R. Dhanganjeyan, Y. P. MilevP, M. A. Kron, M. G. Nair, 'Synthesis and activity of substituted anthraquinones against a human filarial parasite, Brugia malayi', *J. Med. Chem.* **2005**, *48*, 2822-2830.

[18]G. D. Graves, R. Adams, 'Trihydroxy-methyl-anthraquinones. Journal of the American Chemical Society', *J. Am. Chem. Soc.* **1923**, *45*, 2439-2455.

[19]C. T. Huang, C. Y. Huang, Y. C. Hseih, C. H. Chang, A. B. Velu, Y. C. He, Y. L. Huang, T. A. Chen, T. C. Chen, C. Y. Lin, Y. C. Lin, S. R. Shih, A. Dutta. 'Effect of aloin on viral neuraminidase and hemagglutinin-specific T cell immunity in acute influenza', *Phytomedicine*. **2019**, *64*, 152904.

[20]S. W. Tsang, Z. X. Bian, 'Anti‐fibrotic and Anti‐tumorigenic Effects of Rhein, a Natural Anthraquinone Derivative, in Mammalian Stellate and Carcinoma Cells', *Phytotherapy Research*. **2015**, *29*, 407-414.

[21]Q. Z. Ma, Y. Q. Ding, Z. Q. Wu , Y. Li, 'Antitumor effects of emodin in CACO-2 human colon carcinoma cells are mediated via apoptosis, cell cycle arrest and downregulation of PI3K/AKT signalling pathway', *J BUON*. **2018**, *23*, 587-591.

[22]G. Pistritto, D. Trisciuoglio, C. Ceci, A. Garufi, G. D'Orazi, 'Apoptosis as anticancer mechanism: function and dysfunction of its modulators and targeted therapeutic strategies', *Aging.* **2016**, *8*, 603-619.

[23]J. Y. Jang, Y. J. Kang, B. Sung, M. J. Kim, C. Park, D. Kang, H. R. Moon, H. Y. Chung, N. D. Kim, 'a novel topoisomerase iota inhibitor, induces cell cycle arrest and apoptosis via a rosdependent DNA damage signaling pathway in ags human gastric cancer cells', *Molecules.* **2018**, *24*, 96.

[24]Y. Z. Jin, H. N. Sun, Y. Liu, D. H. Lee, J. S. Kim, S. U. Kim, B. Y. Jiao, Y. H. Han, M. H. Jin, G. N. Shen, D. S. Lee, T. Kwon, D. Y. Xu, Y. Jin. 'Peroxiredoxin V Inhibits Emodin-induced Gastric Cancer Cell Apoptosis via the ROS/Bcl2 Pathway', *In Vivo*. **2019**, *33*, 1183-1192.

[25]J. Stanicova, V. Verebova, J. Benes. *In Vivo.* 'Interaction of a Potential Anticancer Agent Hypericin and its Model Compound Emodin with DNA and Bovine Serum Albumin', *In Vivo.* **2018**, *32*, 1063-1070.

[26]J. Esfahlan, V. Panahi-Azar, S. Sajedi, 'Spectroscopic and moleculardocking studies on the interaction between N-acetyl cysteine and bovineserum albumin', *Biopolymers.* **2015**, *103*, 638-645.

[27]M. K. Siddiqi, P. Alam, S. K. Chaturvedi, S. Nusrat, M. R. Ajmal, A. S. Abdelhameed, R. H. Khan, 'Investigating the site selective binding of busulfan to human serum albumin: biophysical and molecular docking approaches', *Int. J. Biol. Macromol.* **2018**, *107*, 1414-1421.

[28]P. K. Suresh, D. Naik, N. Shah, R. Rajasekaran, 'Phenytoin-Bovine serum albumin interactions-modeling plasma protein-drug binding: A multi-spectroscopy and in silico-based correlation', *Spectrochim. Acta, Part A.* **2018**, *193*, 523-527.

[29]P. L. Koen, Kuijpers, C. Bottecchia, D. Cambié, D. Koen, N. J. König, T. Noël, 'A Fully Automated Continuous ‐ Flow Platform for Fluorescence Quenching Studies and Stern ‐ Volmer Analysis', *Angew. Chem. Int. Ed. Engl*. **2018**, *57*, 11278-11272.

[30]D. Raghav, S. Mahanty, K. Rathinasamy, 'Biochemical and toxicological investigation of karanjin, a bio-pesticide isolated from Pongamia seed oil', Pestic. *Biochem. Physiol.* **2019**, *157*, 108-121.

10.1002/cbdv.202000328

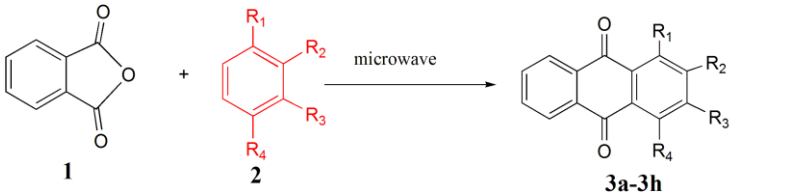

	R_1	R_2	R_3	R_4
3a	H	CH3	H	H
3b	H	CH3	CH3	H
3c	CH3	H	H	CH3
3d	H	OH	H	H
3e	OH	H	OH	H
3f	OH	CH3	OH	H
3g	H	H	H	H
3h	H	Cl	H	H

Scheme 1. Synthesis of a series of anthraquinone derivatives

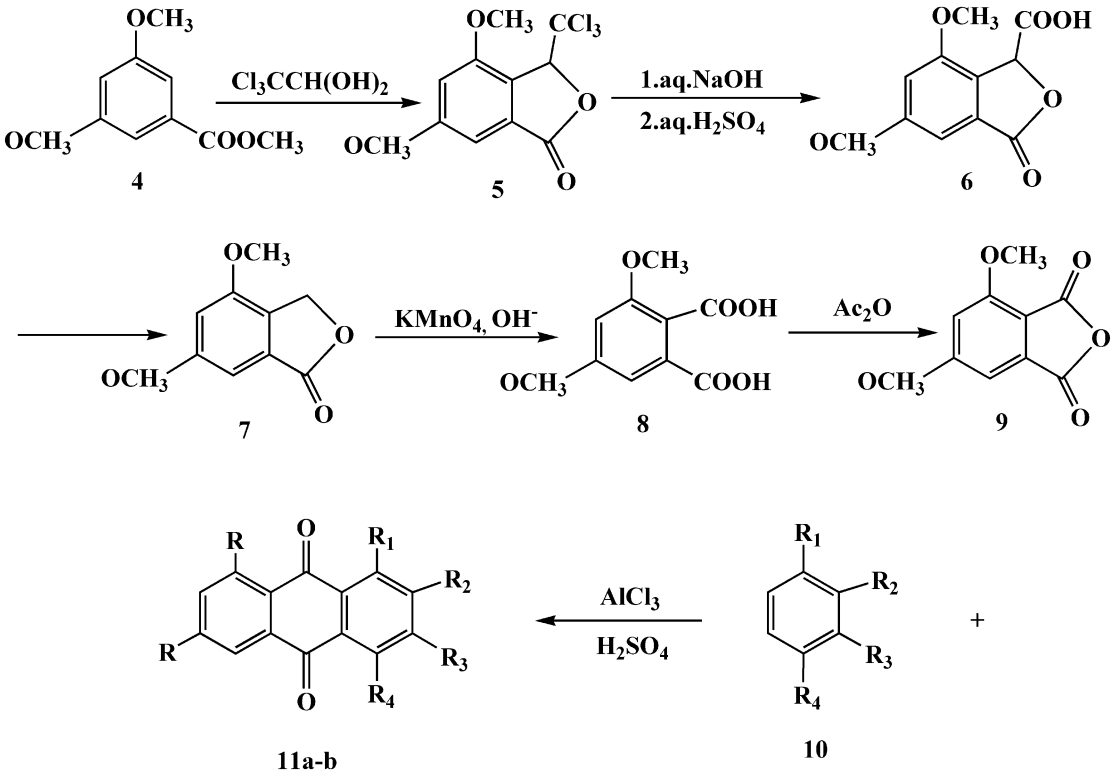

	R	R_1	R_2	R_3	R_4
11a	OH	OH	CH_3	OH	H
11b	OCH_3	OH	H	OH	H
11c	OCH_3	CH_3	H	H	CH3
11d	OCH_3	H	OH	H	H

Scheme 2. Synthesis of 3,5-Dimethoxy-phthalic anhydride and emodin anthraquinone derivatives

10.1002/cbdv.202000328

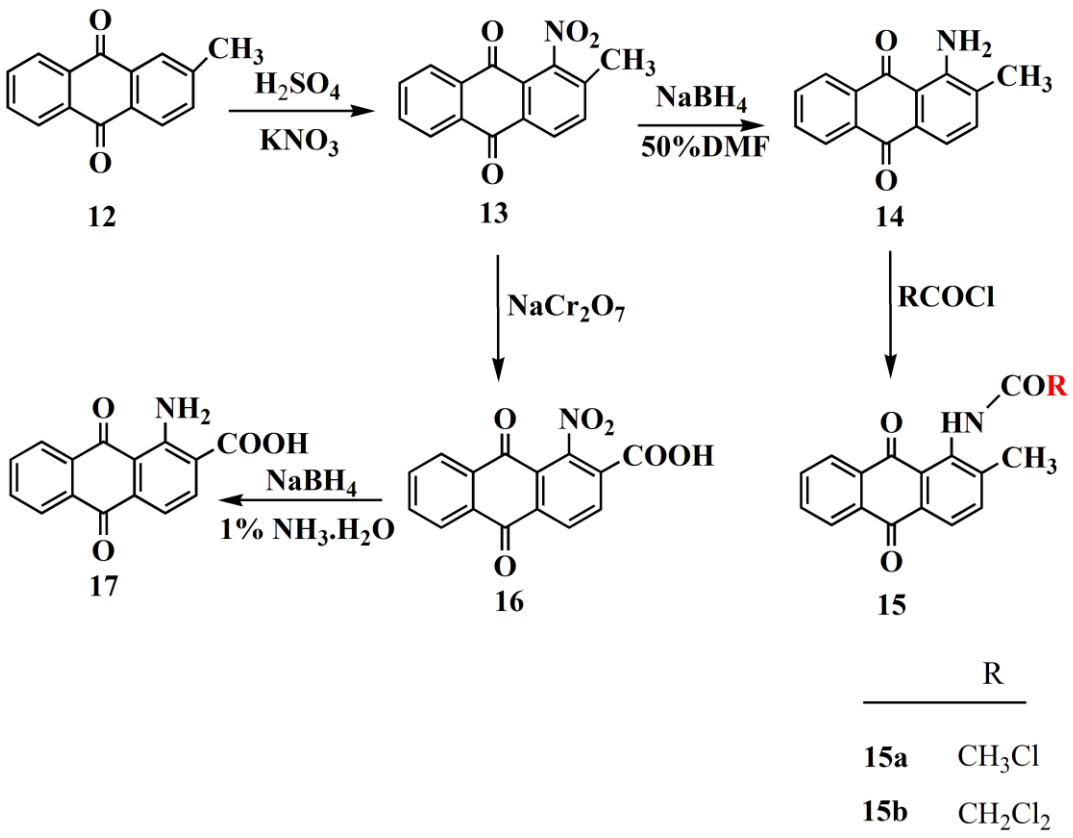

Scheme 3. Synthesis of anthraquinone derivatives

10.1002/cbdv.202000328

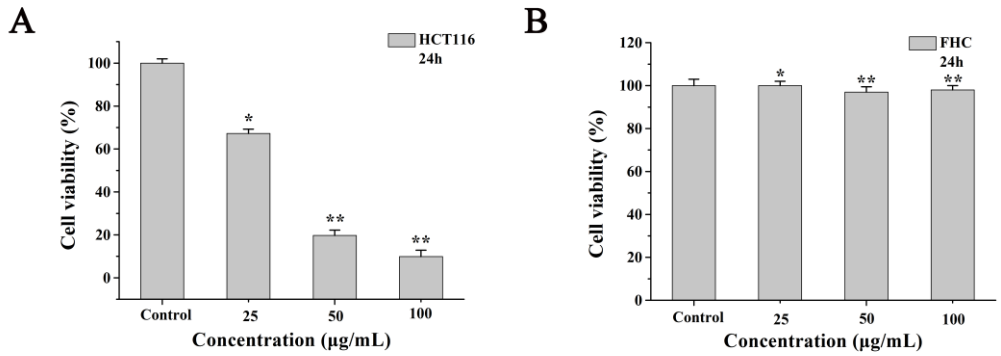

Figure 1. Effect of **11c** compound treatment on the viability of HCT116 and FHC cells. *A)* The effect of **11c** treatment (0, 25, 50, 100 μg/mL, 24 h) on the viability of HCT116 cells was detected using MTT reagent. *B)* The effect of **11c** treatment (0, 25, 50, 100 μg/mL, 24 h) on the viability of FHC cells was detected employing MTT reagent. Significant difference (* p <0.05, ** p <0.01), compared with control group.

10.1002/cbdv.202000328

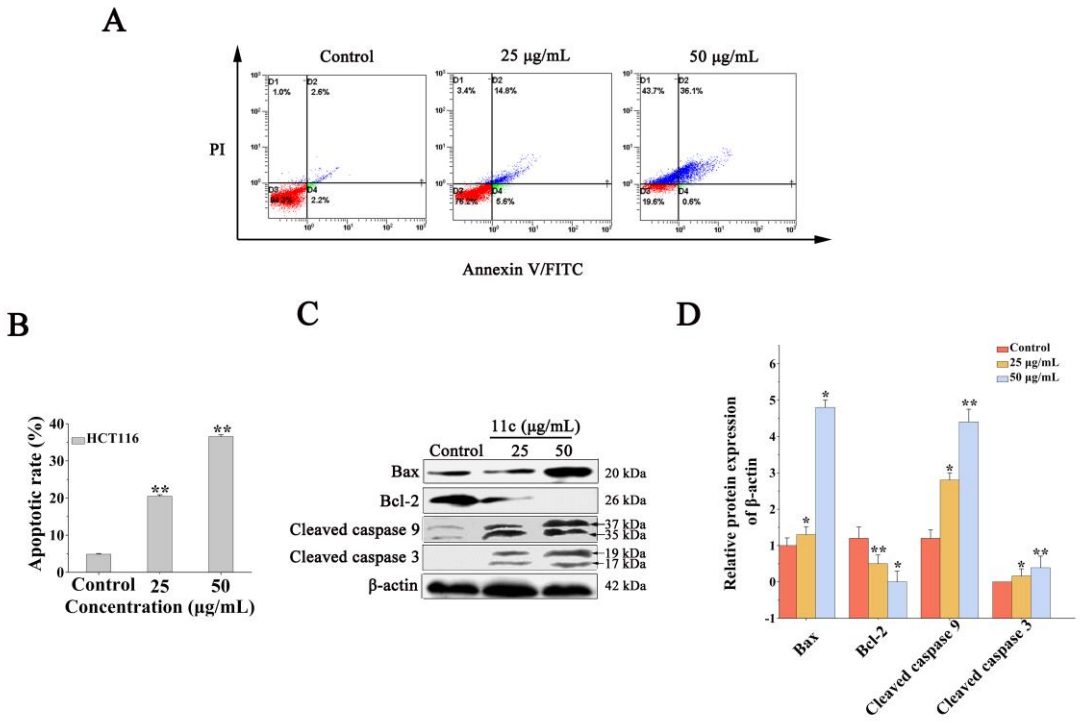

Figure 2. The compound **11c** induces apoptosis to HCT116 cells in a dose-dependent manner. *A)* Flow cytometry was used to detect the apoptosis of HCT116 cells after treatment with **11c** (0, 25, 50 μg/mL, 24 h). *B)* According to the results of flow cytometry, the apoptotic histogram was prepared. The experiment was repeated thrice with significant differences (* p <0.05, ** p <0.01). *C)* Western Blot was performed in HCT116 cells treated with compound **11c** (0, 25, 50 μg/mL, 24 h) to check the expression of apoptosis-related proteins. *D)* A grayscale analysis was performed based on the results of the western blot to obtain a histogram. The experiment was repeated thrice with significant differences (* p <0.05, ** p <0.01), compared with control group.

10.1002/cbdv.202000328

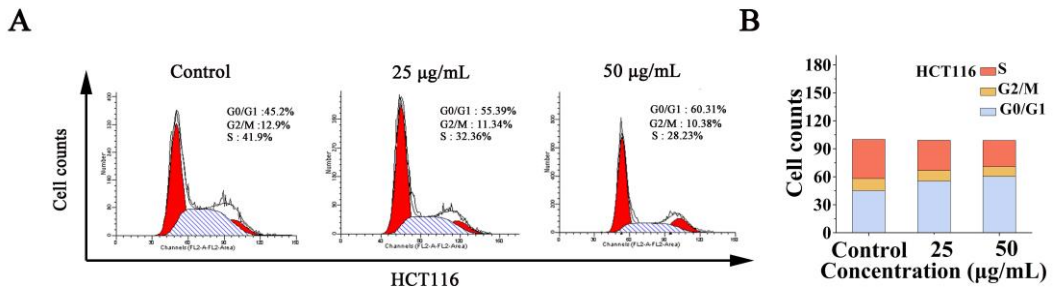

Figure 3. The treatment of compound **11c** leads to cell cycle arrest in G0 / G1 phase of HCT116 cells. *A)* HCT116 cell cycle arrest was detected by flow cytometry upon treatment with compound **11c** (25-50 µg/mL, 24 h). *B)* Histogram analysis showing the cell distribution in different phases of cell cycle. The experiment was repeated thrice with significant differences (* p <0.05, ** p <0.01).

10.1002/cbdv.202000328

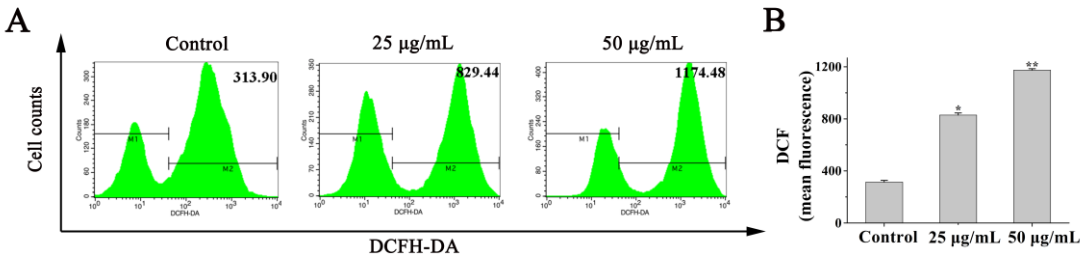

Figure 4. The treatment of **11c** enhances the ROS level in HCT116 cells. *A)* Determination of ROS production in HCT116 cells treated with **11c** (0, 25, 50 μg/mL, 24 h) using flow cytometry. *B)* A corresponding bar graph based on the fluorescence values. The experiment was repeated thrice with significant differences (* p <0.05, ** p <0.01).

10.1002/cbdv.202000328

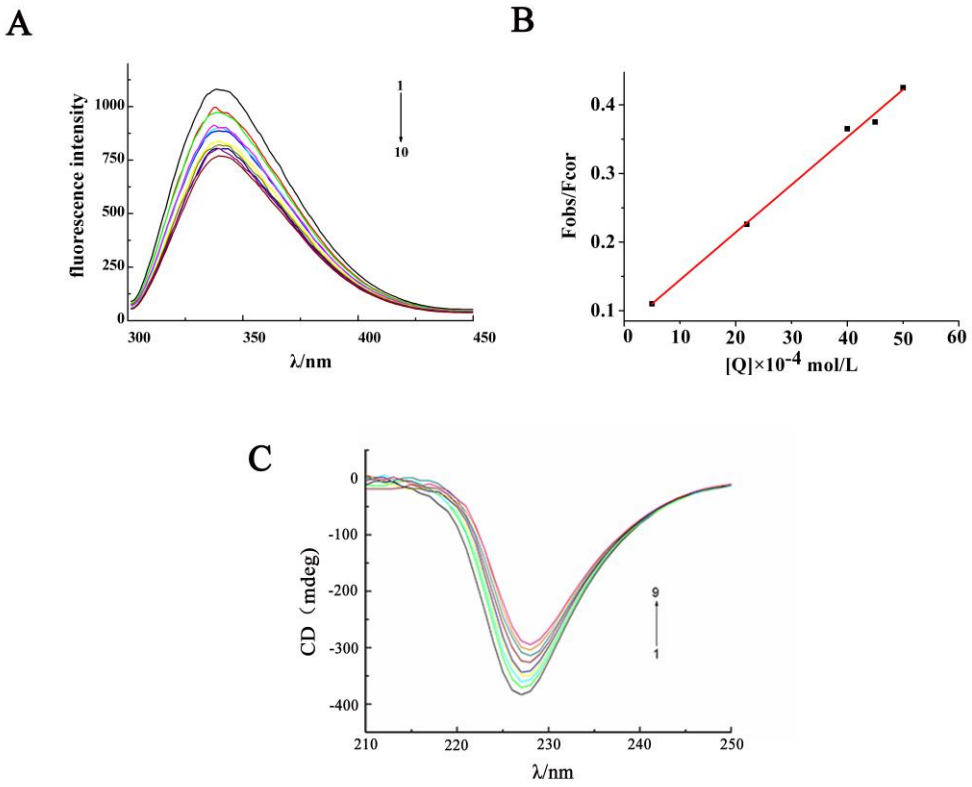

Figure 5. Interaction between the compound **11c** and BSA *A)* Compound **11c** quenched the fluorescence of BSA. C_{BSA}=1.0×10^{-6} mol/L； C_{11c}=1.0×10^{-4} mol/L; T=297K *B)* Stern-Volmer fluorescence quenching curve of **11c** versus BSA system. *C)* The effect of **11C** on the CD spectrum of BSA. C_{BSA}=1.0×10^{-6} mol/L； C_{11c}=1.0×10^{-4} mol/L; T=298.15K

10.1002/cbdv.202000328

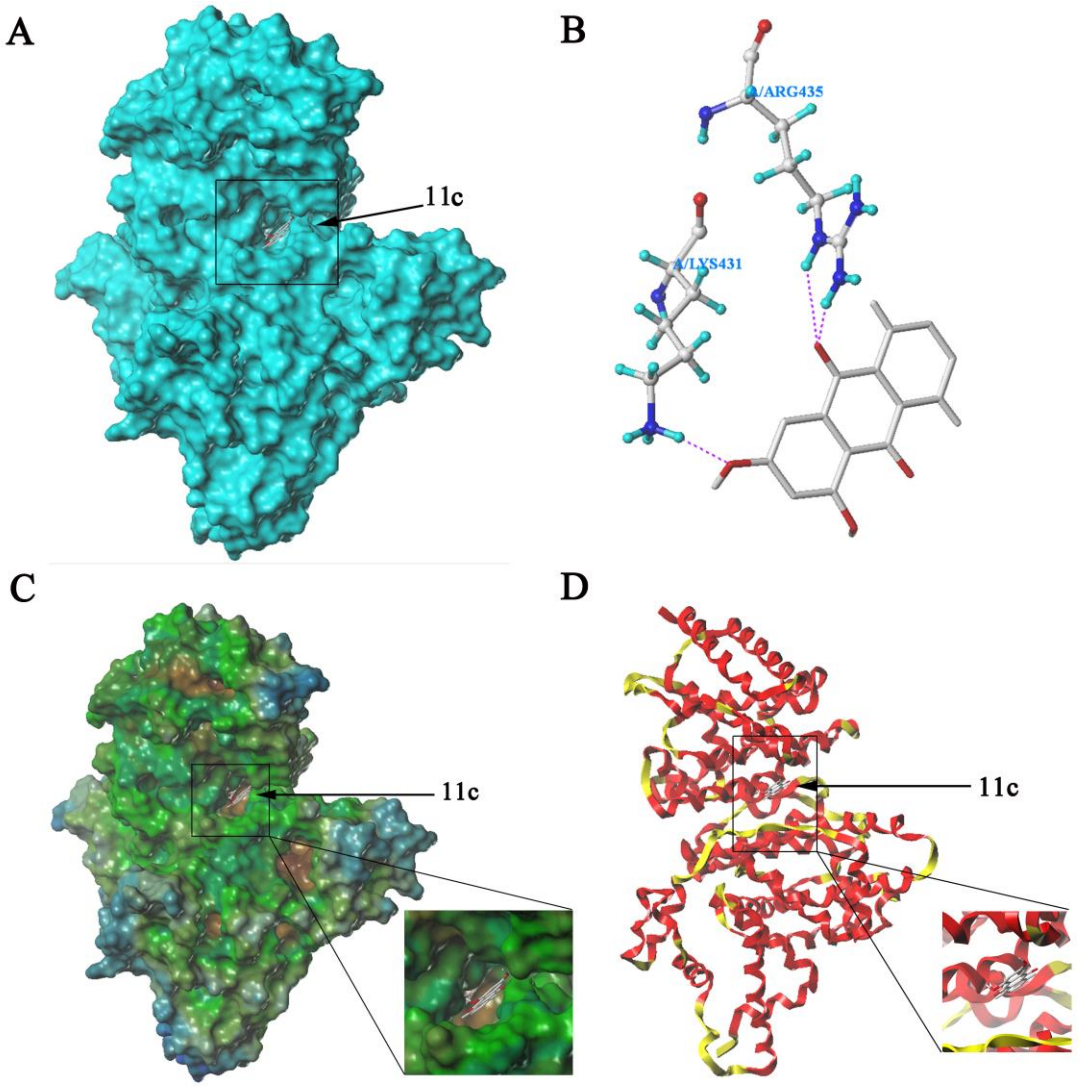

Figure 6. Molecular docking between **11c** and BSA molecules. *A)* **11c** binds to BSA. *B)* **11c** forms hydrogen bonds with BSA. *C)* **11c** binds to BSA hydrophobic site. *D)* **11c** binds to BSA secondary structure.